International Conference on Space Optics—ICSO 2022

Dubrovnik, Croatia

3–7 October 2022

Edited by Kyriaki Minoglou, Nikos Karafolas, and Bruno Cugny,

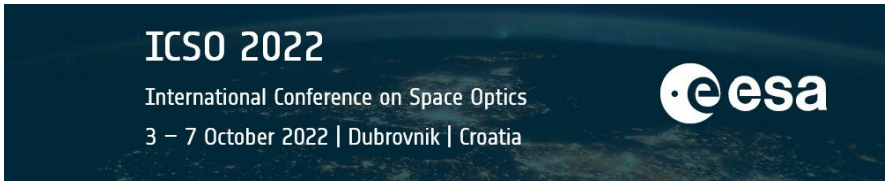

Efficient stray light characterisation: a white light interferometry-based method

International Conference on Space Optics — ICSO 2022, edited by Kyriaki Minoglou, Nikos Karafolas, Bruno Cugny, Proc. of SPIE Vol. 12777, 1277759 · © 2023 ESA and CNES · 0277-786X · doi: 10.1117/12.2690994

Efficient stray light characterisation: a white light interferometry-based method

Ralph Snel[a], Bart Speet[a], Niels Dijkhuizen[a], Gerard Otter[a], Geert Slegtenhorst[a], Micael Miranda[b], Volker Kirschner[c]
[a]TNO, Stieltjesweg 1, 2628 CK Delft, the Netherlands; [b]ATG Europe BV, Huygensstraat 34, 2201 DK Noordwijk, the Netherlands, [c]European Space Agency, Keplerlaan 1, 2200 AG Noordwijk, the Netherlands

ABSTRACT

Stray light is light that reaches the detector that is coming from sources other than the intended observed scene and is one of the main limiting factors for the performance of Earth Observation Space Optical Instruments. It often sets a working limit on the dynamic range of the system limiting the signal-to-noise ratio and minimizing the contrast between a bright and dark scene. Therefore, there is a need for detailed knowledge of the stray light behaviour of the instrument in order to correct the stray light effects in space instruments as much as possible. Characterising stray light to a high level of detail can be a lengthy task involving detailed scans requiring tuneable lasers or other sources of monochromatic light. This work presents a new method for Space Optical Instrument stray light characterisation based on White Light Interferometry.

The characterisation method consists of a broadband light source that passes through a White Light Interferometer to generate spectral fringes in the exiting beam. This light is coupled to an illuminator to the instrument under test. Using the interferometer, Optical Path Difference step-scans are made for each of the spatial points in the instrument field of view. The corresponding interferograms of each illuminated detector pixel contain the full spectral information of direct- and / or stray light reaching that pixel. The dynamic range in the spectral information is increased by multiple exposure levels that are combined to result in high dynamic range spectra. Combining interferometer and spatial scans, the full spectral and spatial sensitivity of each pixel can be determined. This is demonstrated in this paper. The dynamic range in the resulting stray light kernels is shown to exceed seven orders of magnitude, limited only by the optical flux on the detector.

To verify the method a dedicated high-contrast scene was used. The same scene is synthetically constructed out of the stray light characterisation data determined with the interferometric method and is compared with the measured verification scene. Differences in stray light between the measured and synthetic verification scene varied over the instrument detector on the order of 0.1% or less close to the bright part of the scene.

The study shows that the white light interferometer based stray light characterisation is a promising alternative to the traditional methods involving monochromatic sources. The stability of the white light interferometer can be controlled to such level that accurate measurements are possible.

Keywords: Stray light, space optical instruments, white light interferometer

1 INTRODUCTION

At TNO in the space instrument calibration group we have two overarching goals: *self-calibrating instruments*, and *calibration in a day*. This study on efficient stray light calibration, funded by ESA, aims to work towards the latter goal, focussing on the generally time-consuming and hardware-wise expensive stray light calibration of space instruments.

Stray light is one of the main limiting performance factors of space optical instruments for Earth Observation (EO). The gap between state-of-the-art instruments and the stray light levels required by the retrieval algorithms is around one to two orders of magnitude [1], [2]. Measures to avoid or minimize the stray light are taken throughout all development phases of an optical instrument from design to component manufacturing and from performance verification to instrument characterisation. While improvements on existing methods have been demonstrated, further developments are needed to define cost- and schedule effective solutions in the verification and characterisation of stray light in those instruments. Careful characterisation of stray light, coupled with powerful, fast and accurate correction algorithms, can bridge the gap between actual instrument performance and the required stray light suppression. This paper evaluates the existing stray

light performance characterisation and verification methods and demonstrates the feasibility of a new method based on white light interferometry that answers a mission's needs from the technical as well as low cost and fast schedule perspective.

The White Light Interferometer (WLI)-based stray light characterisation method is demonstrated using a Space Optical Instrument (SOI), a breadboard hyperspectral imager instrument representative for Earth Observation instruments in the 300 nm to 500 nm wavelength range. The validity of the characterisation data is verified with a dedicated measurement using a spatially and spectrally confined white light scene, sensitive to instrumental stray light effects.

2 METHODS

A prerequisite for stray light correction is knowledge of the instrumental stray light. The amount of information needed for this could be very large: ignoring polarisation, instrument linearity, electronic crosstalk and hysteresis effects, and photon arrival time effects, there still remains the spectral and spatial information of the observed scene that can affect the stray light of the instrument. Also ignoring one of the two spatial dimensions this leaves one spectral and one spatial dimension to consider for stray light of an imaging spectrometer. This implies that for each instrument detector pixel a 2-dimensional instrument response needs to be known. The two dimensions are the spectral and spatial dimension, with all other potential dependencies ignored. The spectral and spatial range and resolution can be chosen arbitrarily and do not have to match that of the instrument but should ideally cover and distinguish all relevant stray light features to allow correction of the instruments' operational measurements at sufficient accuracy. If one would choose the same range and sampling as the spectral and spatial dimensions of the instrument, this would require knowledge of the stray light of each detector pixel at the same resolution and sampling as the instrument itself. Thus, for an instrument with e.g., 200 spatial and 2000 spectral pixels, 400 000 spatial and spectral data points per detector pixel need to be known.

One way to characterise the stray light response of an instrument is to scan a monochromatic point source through the spectral range and spatial field of view of the instrument, requiring at least 400 000 measurements in the above example. This requires a tuneable monochromatic source with sufficient power, spectral range and spectral resolution, e.g., a tuneable laser. Such lasers exist but are costly and in practice turn out to have significant overhead for a wavelength step, typically on the order of half a minute [3].

An alternative solution is to use a white light interferometer (WLI), e.g., a Michelson interferometer and illuminate the instrument with white light point source, spectrally modulated by the interference fringes, generated by setting the interferometer at a specified Optical Path Difference (OPD). An OPD scan is made instead of a wavelength scan, resulting in the instrument recording interferograms as function of OPD, which after Fourier transformation yield the spectral response of the instrument detector pixel in question. Using the external interferometer, every pixel of the instrument is turned into a Fourier transform spectrometer that measures the combined spectral response of a white light source, the interferometer, and the instrument under investigation. The measured interferogram of each instrument pixel is transformed into a spectrum using the Fourier transform. The thus obtained spectral response of a directly illuminated pixel corresponds to the Instrument Spectral Response Function of that pixel and can be used to scale the measured spectral response of pixels that are not directly illuminated and thus by definition affected by stray light. Using the WLI and the Fourier transform, we have effectively created a tuneable monochromatic light source.

Some advantages of the WLI are simultaneous measurement of an arbitrary wavelength range and arbitrary spectral resolution of the measurements, both beyond the design parameters of the instrument if so desired. Commercial off-the-shelf interferometers are readily available and have OPD scan rates that are fast enough to make the OPD step overhead small enough to be negligible compared to the overall measurement time of an OPD scan (20 ms per step for the WLI used in this study [4]).

3 IMPLEMENTATION

The WLI-based stray light characterisation was implemented by means of a spatial point source of spectrally modulated white light passed through a multi-mode fibre and fed to the SOI by means of an off-axis parabola, with baffles to suppress stray light of the set-up. The angle under which the SOI is illuminated by the collimated beam can be adjusted in the plane of the length of the entrance slit of the SOI. As "instrument under test", the Tropolite instrument [5] was chosen. A Bruker Vertex 80v Fourier transform spectrometer with fibre coupler output was used as light source, using the internal quartz tungsten halogen lamp.

Proper baffling of potential stray light of the set-up and environment was implemented, Figure 3-1, Figure 3-2.

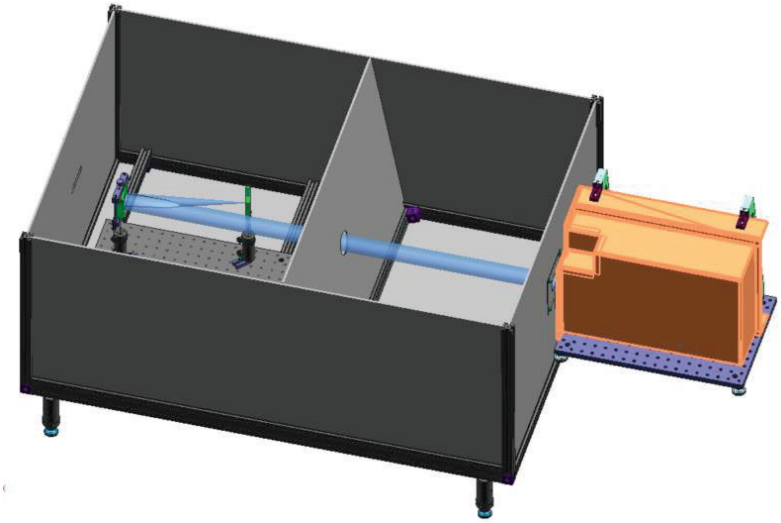

Figure 3-1. CAD model of the overall design of the straylight characterisation setup showing the TROPOLITE instrument in orange on its breadboard

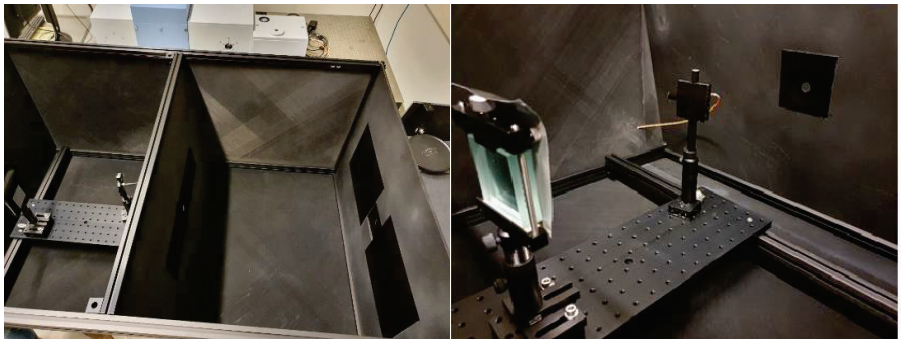

Figure 3-2 Straylight characterisation setup showing the inside of the enclosure with the illuminator, field stop and off-axis parabolic mirror.

A small selection of field angles was chosen for characterisation, matched to a verification scene that was used for verification of the stray light characterisation method. For each field angle, at least two different sets of measurements were made: an OPD scan without saturation in any of the detector pixels, and an OPD scan with 100 times longer exposure time, resulting in saturation of a significant part of the directly illuminated pixels, but also providing much better signal to noise ratio data in the pixels only affected by stray light. An OPD scan consisted of about 3400 unique OPD positions performed in step-scan mode, asymmetrically bracketing the zero path difference position. The OPD scan range was chosen to obtain a spectral resolution in the final result roughly matching that of the SOI. The OPD step size was ¼ of the wavelength of the Bruker He-Ne laser. During the OPD scan, the SOI continuously obtained measurements at a rate of about 6 samples per OPD step. This allowed selection of measurements that were not affected by motion of the interferometer mirror during the integration time of the SOI.

4 ANALYSIS METHOD

Consider a measured signal $I[i, j, k, \alpha_m, t_{exp}]$ at the detector. $[i, j]$ are the detector column- and row identification indices, respectively, k is the index number for detector image read-out, and is coupled to the OPD of the interferometer, α_m is the angle at which the SOI is illuminated (for an integer number m individual angles), and t_{exp} is the exposure time used to record the images. The OPD position x is coupled to the OPD step index number l, where $x = x_0 + l \cdot \delta x$, l is an integer number equal to or greater than 0, x_0 is the OPD position at $l = 0$, and δx is the OPD step size, approximately 158.2 nm

or ¼ of the wavelength of a He-Ne laser. The detector read-out index number k and the OPD step index number l are both integer numbers, but the rate at which k increases is approximately 6 times larger than that at which l increases, resulting in oversampling of the OPD steps in time with the detector read-out.

For each detector pixel $[i,j]$, two measured interferograms $I[i,j,k,\alpha_m,t_{short}]$ and $I\left[i,j,k,\alpha_m,t_{long}\right]$are available, one with short exposure time t_{short}, and one with long exposure time t_{long}. For t_{long}, saturation may occur, the interferograms ($I[k]$) for these pixels will be discarded during processing.

The analysis is performed on a per-pixel basis, complemented with information obtained from detector image level processing. Processing of the data is done as follows:

1. Select a measurement data set $I\left[i,j,k,\alpha_m,t_{exp}\right]$ with given exposure time t_{exp} and viewing angle α_m of the instrument. Read all the data into memory into a 3-dimensional data cube $I[i,j,k]$: field angle i (detector columns), spectrometer wavelength j (detector rows), and detector read-out index number k (time, OPD).
2. Using the differences between subsequent images in time $I[i,j,k+1]-I[i,j,k]$, asses where the OPD steps take place. We know from instrument design that these are simultaneous for all pixels $[i,j]$. Select a single image after an OPD step (identified by a large change in $I[k+1]-I[k]$), picking the image that has least difference with the previous image, ensuring that the interferometer scan mirror was stable. This reduces the data cube to about 3400 images, equidistantly spaced in OPD (assuming proper stepping of the interferometer). This effectively substitutes the detector read-out index number k by the OPD step index number l, resulting in a measurement data set $I\left[i,j,l,\alpha_m,t_{exp}\right]$.
3. For each detector pixel $[i,j]$, check whether saturation occurs during any of the OPD steps l of $I\left[i,j,l,\alpha_m,t_{long}\right]$. Store this information as the saturation map $S[i,j,\alpha_m]$.
4. At each OPD position l, integrate the detector signal $I[i,j]$ over an illuminated unsaturated part of the detector, giving a "white light" interferogram $I[l]$ with a well-defined centre burst because of the broadband spectrum. Identify the location of the centre burst l_0, shift the interferogram $I[l]$ to near-zero OPD $I[l']=I[l-l_0]$, and calculate the Fast Fourier Transform of the interferogram $I[l']$ to obtain a (complex) spectrum $P[\omega]$ as function of wavenumber ω. Residual phase errors will result in a non-negligible imaginary part of the spectrum. Use the real part and imaginary part of the spectrum to determine the residual phase error and correct for it [[6]]. Use the same phase correction for all $[i,j]$ recorded interferograms $I[i,j,l]$ in this OPD scan.
5. For each spectrometer detector pixel $[i,j]$, calculate the Fourier transform $P[i,j,\omega]$ of the interferogram $I[i,j,l]$ with phase correction. Interpolate the spectrum $P[i,j,\omega]$ to the desired wavelength grid (from ½ the wavelength of a He-Ne laser, to approximately 1100 nm in this case), converting from wavenumber ω to wavelength λ, yielding $P\left[i,j,\lambda,\alpha_m,t_{exp}\right]$. The wavelength range extends beyond that of the spectrometer, allowing detection of out-of-spectral-band stray light, if present. This results in a set of analysis results that has the same properties as if the instrument was scanned with a monochromator or tuneable laser. We will call these data sets point source response functions $P\left[i,j,\lambda,\alpha_m,t_{exp}\right]$.

These analyses are done for all measurements, resulting in 9 angular (α_m) times 2 exposure time (t_{exp}) data sets. Next, a High Dynamic Range (HDR) data set is composed for each angle α_m:

A. Take the point source response functions $P\left[i,j,\lambda,\alpha_m,t_{exp}\right]$ for a single angle α_m and both short and long exposure times, as well as the exposure time values t_{short} and t_{long}, and the saturation map $S[i,j,\alpha_m]$ determined in step 3 above. Divide the point source response functions by the corresponding exposure time to obtain integration time normalised point source response functions: $P_n\left[i,j,\lambda,\alpha_m,t_{exp}\right]=P\left[i,j,\lambda,\alpha_m,t_{exp}\right]/t_{exp}$.

B. For each detector pixel, check whether saturation was present in any of the measurements using the saturation map $S[i,j,\alpha_m]$. If saturation was present, select the spectrum obtained with the short exposure time, if no saturation was present, select the spectrum obtained with the long exposure time. This will result in HDR point source response functions:

$$P_{HDR}[i,j,\lambda,\alpha_m]=\begin{cases} P_n[i,j,\lambda,\alpha_m,t_{short}]\ if\ S[i,j,\alpha_m]\ is\ set \\ P_n\left[i,j,\lambda,\alpha_m,t_{long}\right]\ if\ S[i,j,\alpha_m]\ is\ not\ set \end{cases}$$

C. For each monochromatic wavelength λ in the spectra of the response functions $P_{HDR}[i,j,\lambda,\alpha_m]$, extract the corresponding 2-dimensional detector image $P_{HDR}[i,j]$. Identify and select the directly illuminated pixels $[i_{illum}, j_{illum}]$, and integrate the signal $P_{HDR}[i_{illum}, j_{illum}]$ of these pixels. Then divide all pixel values in the image by this integral, resulting in HDR intensity-normalised point source response functions:

$$K_{HDR}[i,j,\lambda,\alpha_m] = \frac{P_{HDR}[i,j,\lambda,\alpha_m]}{\sum P_{HDR}[i_{illum}, j_{illum}, \lambda, \alpha_m]}$$

Since there may be wavelengths where the detector does not record any direct signal, the HDR intensity-normalised point source response functions are spectrally limited to the wavelength range where direct signal is detected by the spectrometer. This step removes any spectral dependence of the light source and interferometer.

Finally, a "full" Instrument Response Matrix (IRM) $K_{HDR}[i,j,\lambda,\alpha]$ is composed from nearest neighbour interpolation of the HDR intensity-normalised point source response functions $K_{HDR}[i,j,\lambda,\alpha_m]$ for the 9 measured angles α_m. The IRM is 4-dimensional, consisting of a real-world angular dimension α, a real-world spectral dimension λ, an instrument angular (detector column) dimension i, and an instrument spectral (detector row) dimension j. The IRM $K_{HDR}[i,j,\lambda,\alpha]$ was roughly matched in real world spectral dimension to the wavelength range that the spectrometer is sensitive to, and in real world angular dimension to the angular range covered by the verification measurements.

5 RESULTS

5.1 Stray light characterisation

The Instrument Response Matrix gives the normalised instrument spatial and instrument spectral response to real world spatial and real world spectral quasi-point sources (at the resolution of the measurement). The stray light matrix of the instrument is the IRM minus the direct light, i.e., light from the real world spectral and spatial dimensions that ends up on the intended instrument spectral and spatial pixels.

The real-world spectral range and resolution of the stray light characterisation is determined through the OPD scan step size and range, respectively. These are under control of the operator and not limited by the instrument under investigation, only by the interferometer used to generate the spectral fringes.

The real-world angular dimension of the characterisation is determined by the classical scan of a narrow field source. The angular range and step size are determined by the operator, the angular resolution is determined by the set-up used for the illumination of the instrument.

The instrument spectral and spatial response are fixed and determined by the instrument design, in particular the number of detector pixels. If needed for SNR reasons, spectral- and/or spatial resolution can be sacrificed for reduced noise, by binning spectral and spatial pixels either during or after detector read-out. This reduces the total data volume and may be beneficial for stray light correction calculations.

Figure 5-1 shows two of the characterisation measurements, one with short (10 ms) and one with long (1 s) exposure time. The detector read-out clearly shows the narrow angular (horizontal) range that is illuminated, and the broad spectral (vertical) range coved by the white light source and the instrument.

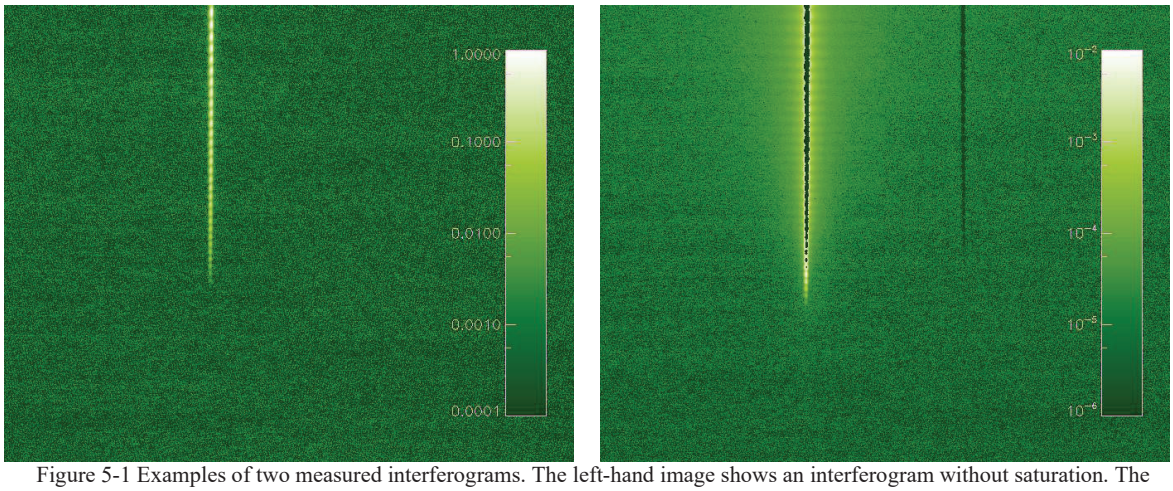

Figure 5-1 Examples of two measured interferograms. The left-hand image shows an interferogram without saturation. The vertical dimension is detector pixel rows, corresponding to the spectral dimension of the instrument, the horizontal dimension is detector pixel columns, corresponding to the angular dimension of the instrument. The bright vertical stripe is the spectrum of the angular point source of white light with superimposed spectral fringes. The right-hand image shows a similar measurement, but with 100 times longer exposure time resulting in saturation in most directly illuminated pixels, but also better signal to noise ratio in the instrumental stray light. The dark vertical band on the right-hand side is detector crosstalk of the bright pixels of the same exposure.

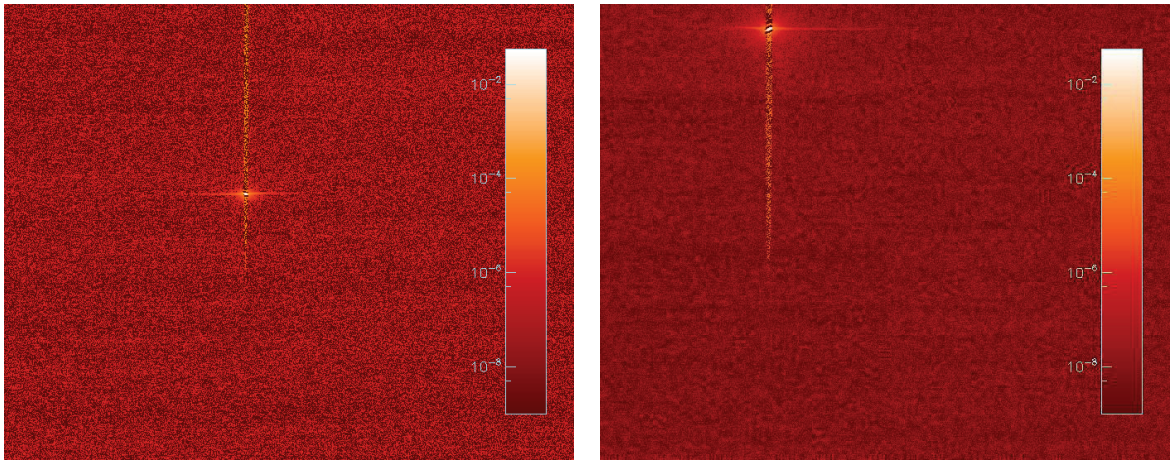

Figure 5-2 Examples of two slices through the instrument response matrix, for all detector pixels, at fixed real world viewing angle and fixed real-world wavelength. The left-hand image shows the IRM for an instrument viewing angle of 89.6 degrees and wavelength of 408 nm, the right-hand image shows the IRM for an instrument viewing angle of 93.8 degrees and wavelength of 472 nm.

Figure 5-2 shows two 2-dimensional slices through the 4-dimensional IRM, showing the detector response derived from the interferograms for two fixed real world instrument illumination angles and real-world wavelengths. Ideally, this should correspond to the instrument response to a monochromatic point source illuminating the instrument. The small bright spot in each image is the expected response, effectively that of the directly illuminated pixels. The horizontal slightly curved line extending from the bright spot is predominantly spatial stray light, likely caused by the optics before the entrance slit of the spectrometer of the instrument. The vertically extending line is increased noise, caused by limitations of the method, likely dominated by OPD noise and shot noise in the interferograms. Only pixels which are directly illuminated (the bright pixels in Figure 5-1 left hand image) are affected, since other pixels have their noise decreased by means of the HDR approach to the measurements and analysis. Figure 5-9 shows the typical noise levels of directly illuminated pixels (blue curve) and pixels that benefit from HDR (black curve).

Figure 5-3 shows two different slices through the IRM, at fixed detector pixel row and column, showing which real-world angle and real-world wavelength contribute to the signal in the pixel. As the number of characterisation angles was limited to 9 in this investigation, there are 9 columns in the images. The spectral range covers 316.4 nm to 516.4 nm. As the angular sampling (Figure 5-5) was chosen to be quite coarse, the resulting figures are correspondingly coarse in that dimension. The characterisation method however allows in principle arbitrary resolution and sampling for these dimensions of the IRM, of course at the expense of measurement time and data volume. Some noteworthy details in Figure 5-3 are the angular (horizontal) extent of the response of the pixels, and the spectrally (vertically) present noise which is more prominent at the angles that generate the direct illumination.

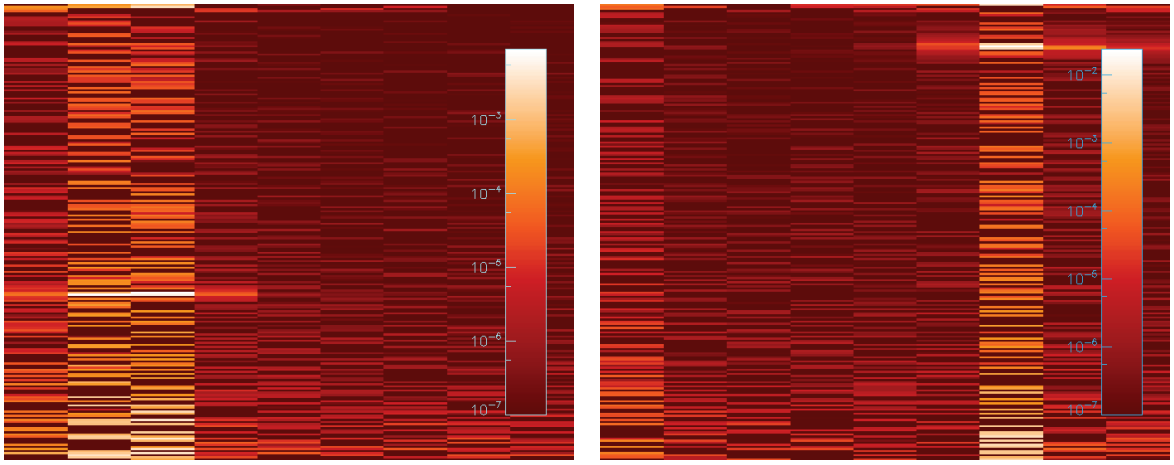

Figure 5-3 Examples of two slices through the instrument response matrix, for all measured real world viewing angles (columns) and all measured real-world wavelengths between 375 and 484 nm (rows), at fixed detector pixel row and column. The left-hand image shows the IRM for detector pixel row 680 and column 580, the right-hand image shows the IRM for detector pixel row 1050 and column 424. The images show, for the given detector pixel, from which direction and which wavelength the light reaches the pixel. The pixel in the left-hand image was chosen to lie between two characterisation angles, the right hand one very close to one of the characterisation angles.

The dynamic range in the IRM is determined on the one hand by the noise properties of the instrument, but also by the number of OPD steps and OPD scan range, and to very strong degree by the exposure levels used to compose the HDR IRM. Provided that the instrument is not adversely affected by over-exposure of parts of the detector, the dynamic range can be arbitrarily extended by including more over-exposed measurements in the characterisation.

The dynamic range of the measurement results obtained in this study is estimated from the noise in the IRM. The total amount of direct light is normalised to unity for each monochromatic point source, which means that the noise in the IRM is also expressed as a fraction of the direct light and can thus be used to estimate the dynamic range. However, as there are typically 77 pixels in the directly illuminated part of the measurements, corresponding to a certain spectral and spatial resolution of the characterisation, the noise-dominated part of the IRM was smoothed with this typical resolution before the dynamic range was determined. Figure 5-9 shows the typical noise level in (smoothed) instrument response matrix data for both pixels benefiting from the long exposure times in the HDR data (black curve) and those that do not (blue curve). The corresponding dynamic range well exceeds 10^7 for the wavelength ranges where both the source is bright, and the throughput of the instrument is high. At wavelengths below 380 nm the instrument optics are opaque due to the glass of the telescope lenses, and at wavelengths above 480 nm the instrument no longer detects direct light as the spectrum no longer falls on the detector.

The minimum measurement time for the characterisation performed in this study depends on the desired spectral resolution, determined by the number of OPD steps needed to obtain the desired spectral resolution, or about 3400 steps for a spectral resolution of 0.5 nm at a wavelength of 500 nm, or 20 cm^{-1}. There will be a minimum time needed to read out the detector, which will set the overall minimum time for an OPD scan. Depending on the brightness of the light source used for characterisation, there will be an additional term to account for the total integration time to collect the required photons. In the case of these measurements and hardware under test, the short exposure measurements were set at 10 ms exposure time and were obtained at slightly over 0.5 seconds per frame. For a full scan of 3400 steps with synchronisation between the interferometer and the spectrometer read-out, this would result in just under 30 minutes. The long exposures at 1000

ms would take slightly over 60 minutes for a full scan. The 9 angles scanned would combine to slightly under 14 hours total acquisition time for the complete set of data presented here. In practice, due to lack of hardware synchronisation between the interferometer and spectrometer, the real measurement time was about a factor 6 longer. In this total measurement time, the stray light properties for the entire input spectral range between 316.4 nm and far into the infrared were characterised, limited by the spectral properties of the light source and the optics of the interferometer, both of which can be configured to cover selections of the wavelength range between 200 nm and about 500 µm.

With a brighter light source (which is a commercially-off-the-shelf option for the interferometer), the exposure time of the measurements can be reduced, resulting in the overall characterisation time to be limited by the overhead of the data acquisition of the instrument, in this study for the acquisition of 3400 * 2 * 9 frames.

5.2 Stray light verification

The verification measurement was performed by scanning the instrument over a pre-defined angular range in a single exposure time. The light source used was a white light source, spectrally limited by a bandpass filter. SNR was improved by repeating the measurement and averaging the result. A matching dark measurement was made, using identical conditions but with the light source blocked. Figure 5-4 (left image) shows the resulting verification scene. The detector rows represent the spectral dimension, with short (UV) wavelengths at the bottom, and long (480 nm) wavelengths at the top. Detector columns represent the angular (spatial) dimension of the scene (Figure 5-5 blue curve). A spatially sharply defined image is expected for a perfect instrument, but due to stray light a loss of contrast close to the sharp edges are expected for a real instrument (Figure 5-7 black curve). Since the bandpass filter has a gradual transition from maximum to minimum transmission, a gentler behaviour of the spectral dimension of the verification scene is expected (Figure 5-6 black curve).

A synthetic verification scene was created by taking the measured verification scene and selecting only those pixels which likely receive direct illumination. Spatially, the steep edges of the curve in Figure 5-7 were used (between pixel columns 405 and 593), spectrally the range between detector rows 600 and 1101 was used (Figure 5-6), which broadly covers the full range where direct light could be present, but also likely covers pixels affected by (spectral) stray light. For each pixel in the specified ranges, the nearest neighbour IRM entry was found in real world wavelength and angle. The 2-dimensional (detector pixel row and column) IRM for this wavelength and angle was shifted to the pixel coordinates of the pixel under investigation, multiplied by the pixel value, and added to the synthetic scene. This resulted in the synthetic verification scene shown in the right hand of Figure 5-4.

The synthetic verification scene of Figure 5-4 shows the same spectral and spatial features as the measured verification scene, in particular the spatial stray light extending to the left and the right of the illuminated part of the scene. Spectrally, a lot of “blocky” noise is present. This is consistent with the angular sampling, nearest neighbour interpolation scheme, and increased noise in the detector spectral dimension of the IRM as shown in Figure 5-2.

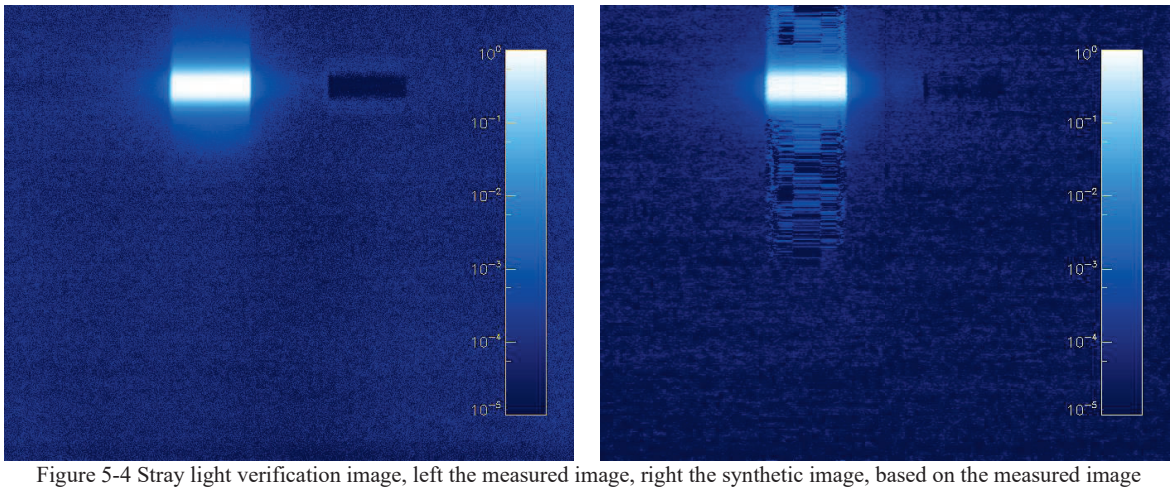

Figure 5-4 Stray light verification image, left the measured image, right the synthetic image, based on the measured image and the characterisation data. The bright spot is a spectrally and spatially confined illumination of the instrument, the dark spot is crosstalk during detector read-out

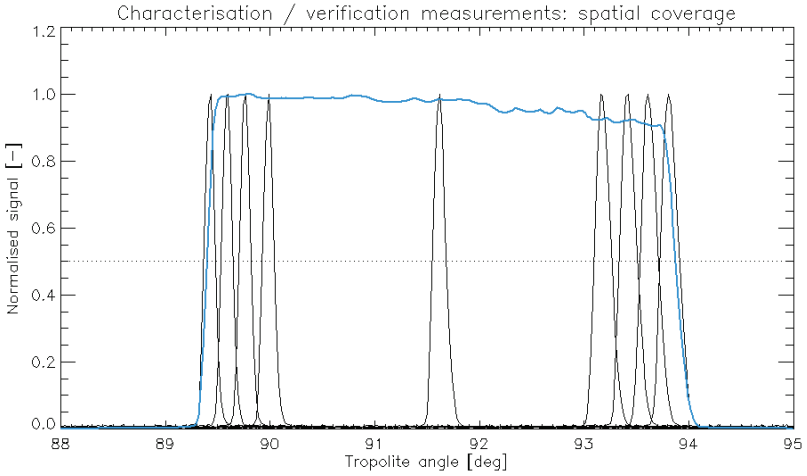

Figure 5-5 The angular coverage of the characterisation measurements (black) and the verification scene (blue)

Quantitatively, the measured and synthetic verification scenes are compared by means of integration over parts of the detector spectral or spatial dimensions. Figure 5-6 shows the spatially integrated scenes revealing the average spectral profiles of the measured (black) and synthetic (blue) verification scenes. Overall, the shape and magnitude agree well. In more detail, the synthetic scene seems to have a slightly higher signal at signal levels below half a percent. This is likely due to actual (spectral) stray light being considered as direct signal and counting twice in the synthetic image, once as direct and once as stray light. At pixel row values below 500, there seems to be a slight underestimate of the stray light by the characterisation.

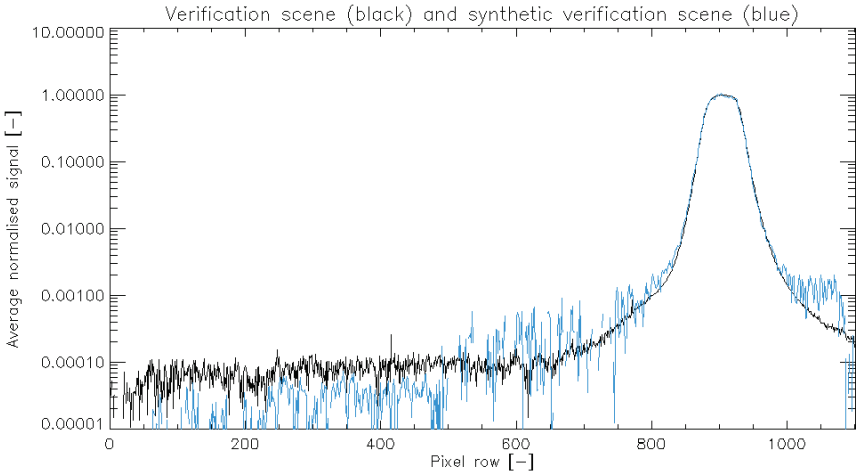

Figure 5-6 The spectral behaviour of the verification scene (black) and the synthetic verification scene (blue), integrated over columns 400 to 599

Figure 5-7 shows the spectrally integrated signals of the measured and synthetic verification scene. The match is quite good down to the 0.05% level, with only a slight over-estimate of the stray light in the synthetic scene around pixel column 600. The noise in the integrated synthetic scene is at the 10^{-4} level, with a slightly lower average signal level than measured. The crosstalk-effect around column 900 is clearly visible in the measured verification data, but less so in the synthetic data. It is, however, still caught to some degree by the characterisation data, resulting in a slightly lower stray light level than adjacent pixel column ranges. As it turns out (data not shown) the crosstalk in the detector is not linear, and the assumption for stray light is that it behaves strictly linearly with the recorded signal after dark correction.

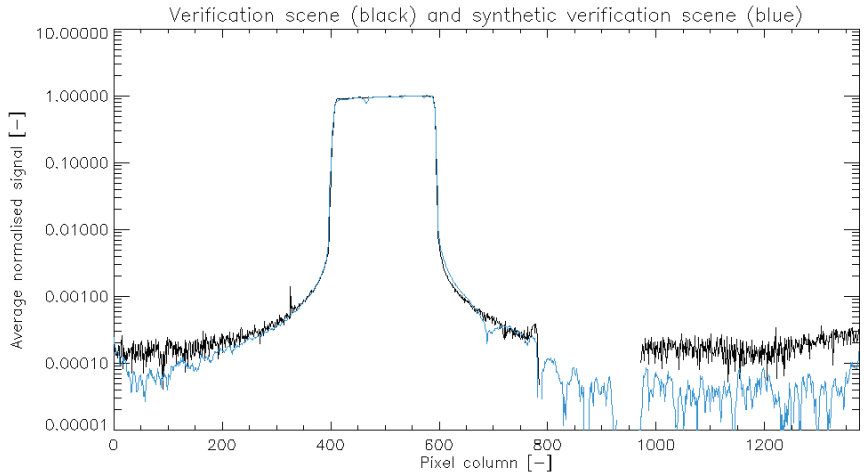

Figure 5-7 The spatial behaviour of the verification scene (black) and the synthetic verification scene (blue), integrated over rows 866 to 944

An interesting region in the verification scene is the part close to the directly illuminated spatial detector columns, which is known to not receive any direct light. This would be columns below 400 and above 600. In these regions, significant amounts of signal are recorded while from the design of the measurement we expect no direct signal to be present. We can thus with confidence state that the recorded signal is dominated by instrumental stray light. The right hand Figure 5-8 shows the spatially integrated signal over columns 600 to 619, in the region where we saw the deviation between measured and synthetic data in Figure 5-7. Spectrally, the match is reasonably good, apart from the peak being over-estimated by about 30% of the stray light, or 0.1% of the level of the direct illumination. The reason for this is not fully understood but could be related to a loss of resolution when convolving the measured scene (already affected by instrumental resolution) with the IRM, also affected by instrumental resolution. The left hand Figure 5-8 shows the spatially integrated signal over columns 375 to 394, basically mirrored in the illuminated part of the verification scene. Here, the match between the measured and synthetic scene is much better and no systematic difference can be discerned.

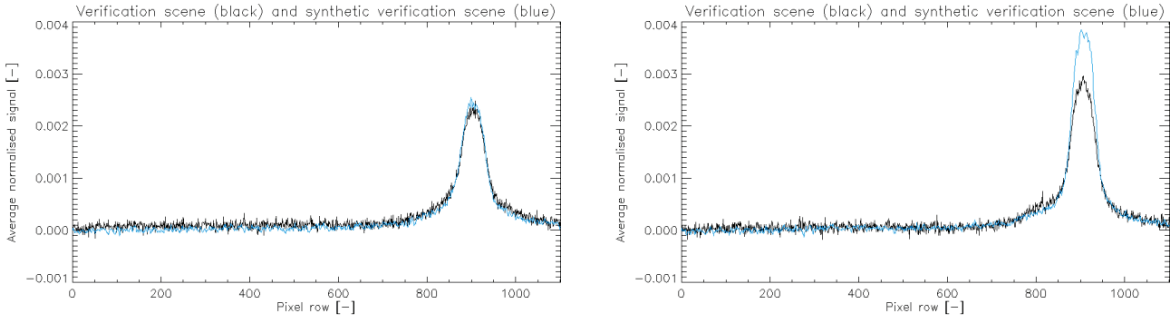

Figure 5-8 Spatially integrated normalised signal of columns 375 and 394 (left) and of columns 600 and 619 (right), just outside of the directly illuminated part of the verification scene. The black curve is the measured signal, the blue curve is the synthetic scene

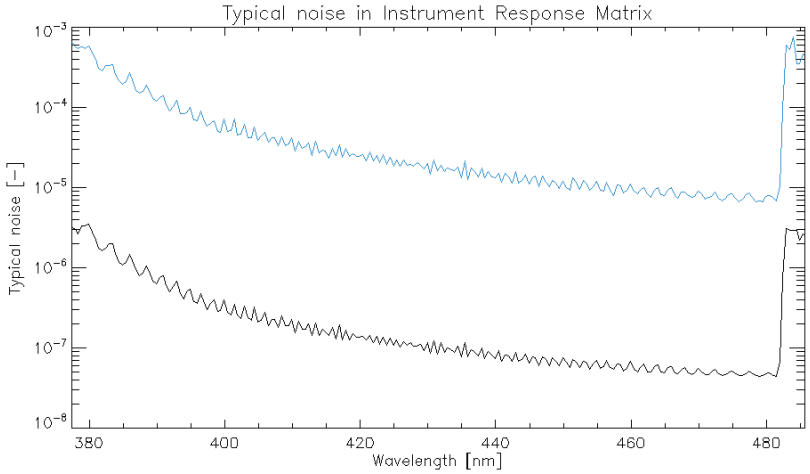

Figure 5-9 Typical noise level in the Instrument Response Matrix for resolution elements that benefit of the HDR (black) and those that do not (blue) due to saturation of the long exposure. The total direct signal is unity, the noise is expressed per pixel with respect to the integrated direct signal. The variation of the noise with wavelength is due to the spectral throughput of the instrument and the spectral brightness of the light source used

5.3 Discussion

The WLI-based stray light characterisation of imaging spectrometers and hyperspectral imagers has some clear advantages over existing (monochromator- or laser-based) methods. In view of the goal to perform space instrument calibration in a single day, the main advantage is the speed of the method: a WLI-based method has a measurement overhead of 20 ms for an OPD step, while the alternative typically has an overhead of tens of seconds per wavelength step. For a typical SOI with 2000 independent wavelength bands of interest, and 200 independent viewing angles of interest, and assuming a viewing angle step overhead of 1 minute and a wavelength step overhead of 30 seconds, and no HDR, the minimum time for characterisation would be 139 days overhead time for wavelength and angle setting. A WLI-based characterisation, with e.g., 5000 OPD steps, would take slightly under 9 hours for measurement overhead alone. To both numbers should be added the actual time to collect the light, and the overhead for reading out the detector. If we assume 0.5 seconds for the sum of these two, the total time needed for characterisation of the SOI using a laser or a WLI, would increase to 141 days or 6 days, respectively.

In addition to the significantly shorter overhead time, other advantages of the WLI-based characterisation are the wavelength calibration of all SOI pixels that can be derived from the characterisation results, and the large wavelength range covered, both in-band for the SOI, but at no extra measurement time, also out-of-spectral-band characterisation. The spectral range and spectral resolution of the characterisation can be set by means of the OPD scan parameters, at nearly arbitrary values, only limited by the light source and optics involved, and the highest spectral resolution that can be provided by the WLI (300 000 in the case of the WLI used in this study). This also allows fast characterisation of the instrument spectral response function of all SOI pixels, especially if the full field of view of the SOI can be illuminated in one go.

The parameters of importance in a WLI-based stray light characterisation are the OPD step size, the OPD scan range, and the number of HDR levels with corresponding over-exposure. The OPD step size determines the spectral range covered, with the shortest wavelength being double the OPD step size. Any wavelengths shorter than this will be aliased to longer wavelength, which can not be distinguished from these longer wavelengths without prior knowledge. The OPD scan range determines the spectral resolution, with a longer scan range resulting in higher spectral resolution. The noise in the interferograms is mostly determined by the noise of the SOI, but also the stability of the WLI affects the interferograms through the OPD noise and light source stability. All noise sources combined will result in a maximum dynamic range in the spectra obtained from the interferograms, as well as a noise floor. The noise floor can be lowered by means of HDR measurements, which can be done arbitrarily much. The OPD noise and shot noise in the interferograms limits the dynamic range in the spectra of pixels that receive direct light, which is one of the main limitations of the method as implemented here.

Potential improvements of the method address the dynamic range of the directly illuminated pixels. By spectrally limiting the number of directly illuminated pixels, e.g., by means of a bandpass filter, fewer pixels are affected by the constraint in the dynamic range of the directly illuminated pixels, allowing better characterisation of purely spectral stray light. This will however be at the expense of additional measurement time.

The validity of the stray light characterisation data was tested with a verification measurement, which was used to compose a synthetic verification measurement from the combined characterisation data. Though affected by noise, the agreement between the synthetic and real measurement is good, also in regions only affected by stray light. The main limitation is the dynamic range in the directly illuminated pixels, resulting in higher noise in the purely spectral direction of the detector than in any other directions. We are currently investigating modifications to the characterisation method to reduce the impact of this limitation.

The stray light characterisation data can be used to feed a stray light correction algorithm, as done e.g., in [1] and [2]. This will allow the SOI to achieve higher spectral and spatial contrast after correction than intrinsically possible by the instrument. The WLI-based stray light characterisation is efficient enough to quickly gather large amounts of data, allowing more detailed correction by the stray light correction algorithms than currently possible with only coarse sampling in real world spectral and real-world angular dimensions.

6 CONCLUSION

A “Space Optical Instrument” hyperspectral imager breadboard in the wavelength range of 380 to 480 nm range was characterised for stray light using a novel white light interferometer-based method for the spectral dimension. The method is very fast compared to existing methods and is more flexible regarding spectral range and spectral resolution. The dynamic range demonstrated here exceeds 10^7 and could easily be extended to even higher ranges. For purely spectral stray light, the dynamic range was limited to a few times 10^5, prompting a follow-up study to improve this. A dedicated verification measurement confirms the validity of the characterisation data at the 0.1% level or better.

The technology readiness level was brough to TRL 4, breadboard functional verification in a laboratory environment. This method contributes to TNO’s space instrument calibration group’s goal to calibrate space instruments in a day.

This work was made possible under ESA contract 4000129143/19/NL/AR.

REFERENCES

[1] Characterization and correction of stray light in TROPOMI-SWIR, Tol *et al*, Atmos. Meas. Tech., 11, 4493–4507, 2018, https://doi.org/10.5194/amt-11-4493-2018
[2] Characterization and correction of stray light in optical instruments, Zong *et al*, Sensors, Systems, and Next-Generation Satellites XI, edited by Roland Meynart, Steven P. Neeck, Haruhisa Shimoda, Shahid Habib, Proc. of SPIE Vol. 6744, 67441L, (2007), https://doi.org/10.1117/12.737315
[3] M^2 SolsTiS Doublet data sheet, Ti Sapphire Laser | CW Narrow Linewidth Laser | SolsTiS | M Squared (m2lasers.com)
[4] High-End Vacuum Research | Bruker
[5] Maresi, Luca & Meulen, Wencke & Vink, Rob. (2014). TROPOLITE, on the path of atmospheric chemistry made simple. 92410J. 10.1117/12.2067473.
[6] Correction of phase errors in Fourier spectroscopy, Porter, C.D., Tanner, D.B., International Journal of Infrared and Millimeter Waves, Vol. 4, No. 2, 1983